Using a pore-scale model to quantify the effect of particle re-arrangement on pore structure and hydraulic properties

Oagile Dikinya,[1,*†] Peter Lehmann,[2,3] Christoph Hinz[1] and Graham Aylmore[1]

Abstract:

A pore-scale model based on measured particle size distributions has been used to quantify the changes in pore space geometry of packed soil columns resulting from a dilution in electrolyte concentration from 500 to 1 mmol l^{-1} NaCl during leaching. This was applied to examine the effects of particle release and re-deposition on pore structure and hydraulic properties. Two different soils, an agricultural soil and a mining residue, were investigated with respect to the change in hydraulic properties. The mining residue was much more affected by this process with the water saturated hydraulic conductivity decreasing to 0·4% of the initial value and the air-entry value changing from 20 to 50 cm. For agricultural soil, there was little detectable shift in the water retention curve but the saturated hydraulic conductivity decreased to 8·5% of the initial value. This was attributed to localized pore clogging (similar to a surface seal) affecting hydraulic conductivity, but not the microscopically measured pore-size distribution or water retention. We modelled the soil structure at the pore scale to explain the different responses of the two soils to the experimental conditions. The size of the pores was determined as a function of deposited clay particles. The modal pore size of the agricultural soil as indicated by the constant water retention curve was 45 μm and was not affected by the leaching process. In the case of the mining residue, the mode changed from 75 to 45 μm. This reduction of pore size corresponds to an increase of capillary forces that is related to the measured shift of the water retention curve.

KEY WORDS pore structure; particle size distribution; particle re-arrangement; hydraulic properties; saturated hydraulic conductivity; soil water retention

INTRODUCTION

Soil hydraulic properties including water retention and hydraulic conductivity are directly related to the geometry of available pore spaces (Vogel and Roth, 2001) and are crucial in the study of water flow and solute transport in soil profiles and soil water availability for plant growth. However, a fundamental problem in studying flow through porous media is the difficulty in characterizing the pore space which controls the complex nature of the displacement mechanisms of fluids (Hunt and Gee, 2002b). Porous media generally consist of interconnected networks of pores including structural pores (100–10 000 μm) and matrix pores (0·1–10 μm), and this large disparity in dimensions poses practical and theoretical challenges to modelling the total system response (Tuller and Or, 2002).

The structure and hydraulic functions of aggregated soil material are not constant but depend on the stability and any re-arrangement of the aggregates. Favourable soil structure is important in enhancing porosity, decreasing erosion (Bronick and Lal, 2005) and improving water storage and movement (Pachepsky and Rawls, 2003). Physical changes due to the break-up of connected capillary-flow paths influence both solute diffusion and water retention characteristics (Hunt and Gee, 2002b). Particle release and re-deposition are complex functions resulting from the nature and interaction of many factors such as soil texture, mineral composition and exchangeable ions (Kay, 1998) as well as electrolyte concentration or ionic strength (Grolimund *et al.*, 1998; Kretzschmar *et al.*, 1999). Irreversible changes in soil structure may occur when clay particles become dislodged when the electrolyte concentration is decreased (Lebron *et al.*, 2001) with mobilized particles being redeposited within the soil matrix (Lebron and Robinson, 2003; Ranville *et al.*, 2005). The total porosity and median pore size generally decrease over time owing to colloidal dispersion (Auset and Keller, 2004), followed by settlement and filling of pore spaces (Leij *et al.*, 2002).

Prediction of hydraulic properties is generally and typically based on models that consider pore-size distribution (Assouline *et al.*, 1998; Arya *et al.*, 1999b; Hwang and Powers, 2003) and generalized formulations include parameters describing pore tortuosity, pore connectivity or pore interaction. Vogel (2000) showed the relevance of

*Correspondence to: Oagile Dikinya, School of Earth and Geographical Sciences, The University of Western Australia, 35 Stirling Highway, Nedlands WA 6009.
E-mail: ogdikinya@hotmail.com; dikinc01@cyllene.uwa.edu.au
† Permanent address: Department of Environmental Science, University of Botswana, Private Bag 0022, Gaborone, Botswana.

pore geometry on flow and transport in a numerical study and also demonstrated the combined effects of pore-size distribution and pore connectivity on the constitutive relations of soil hydraulic properties. Vogel and Roth (2001) used a Euler number to quantify the three-dimensional connectivity of a measured sample and to show the effect of this property on hydraulic properties.

Several models also characterizing water flow at the pore scale have recently been presented (Fischer and Celia, 1999; Vogel, 2000). Flow dynamics through porous media have been studied using fractal models to estimate hydraulic properties from more readily measured soil properties such as texture or structure (Kravchenko and Zhang, 1998; Hunt and Gee, 2002a; Huang and Zhang, 2005). Many attempts have been made to determine hydraulic properties from particle size distribution (Reddi *et al*., 2000; Hwang and Powers, 2003) since the spatial arrangement of particles, particularly in sandy soils, controls the pore structure. However, the spatial arrangement of the particles is particularly important when soil particles are mobilized and re-deposited, when the macro particle size distribution is little affected.

A different approach to the prediction of hydraulic properties is to model the particle configuration and use this to derive the pore network information subsequently. This approach has the advantage that both the particle distribution and the pore-size distributions are considered simultaneously, enabling the effects of particle rearrangement on hydraulic properties to be modelled while leaving the particle size distribution unchanged.

In the present paper, we model the changes of pore structure, which occurred during the leaching of two soils of different structural characteristics using experimentally measured particle size and pore-size distributions during leaching. While the paper aims to elucidate the influence of particle release and re-arrangement on pore structure and hence on hydraulic properties, the mechanisms of particle mobilization and re-deposition are not considered in the context of the proposed model. Thus, the paper focuses on the effect of particle rearrangement on hydraulic properties, (before and after leaching scenarios).

MATERIALS AND METHODS

Soil materials

We used two different soils as porous media, an agricultural soil classified as Vertic Ferralsol (World Reference Base for soil classification, FAO, 1998) and a mining residue or spoil classified as Anthroposol (Soil Taxonomy classification, Soil Survey Staff, 1996), consisting of waste products. The agricultural soil was collected from 'Yalanbee' CSIRO Research station farm near Bakers Hill, Western Australia. The soil is extensively used for cropping throughout the Western Australian wheat belt and provides a classic example of a relatively fragile agricultural soil that is highly susceptible to structural breakdown and permeability problems. The mining residue was collected from the Sandalwood Cable Sands mine site, 5 km north of Brunswick Junction, Western Australia. The mining residue is a completely disrupted and reconstituted material (sand and clay) and presents similar structural problems in the rehabilitation of mining sites.

Particle size distribution measurements

The particle size distributions for the various sized fractions of these porous media were determined using the sedimentation or grain size mechanical wet sieving method (Day, 1965) for the particle size range from 45–2000 μm, while a laser light scattering technique (Mastersizer Microplus Ver.2·18, c/o Malvern Instruments Ltd, 1995) was used for the range <45 μm.

A mixture of air-dried soil (<2 mm) with water was boiled and 6% hydrogen peroxide solution was added to remove organic matter followed by a calgon/NaOH mixture to disperse the soil. Suspensions were collected for various fraction sizes according to the sedimentation theory or Stokes's law (Stokes, 1891). For the sand fractions, suspensions were separated using sieves of various diameters (1000, 500, 250, 125, 45 μm). Suspensions passing through 45 μm together with effluents from subsequent leaching experiments were analysed for particle size distribution using a Malvern Mastersizer analyser. Suspensions were dispersed in the Mastersizer's ultrasonic bath unit (equipped with a small angle light scattering apparatus, Helium–Neon laser; $\lambda =$ of 633 nm, as a light source) for about 25 min. Suspension concentrations were adjusted until an obstruction of a least 0·2% was reached for best results using refractive indices of 1·59 and 1·33, respectively, for clay and deionized water with a particle density of 2·6 g cm^{-3}. Both values were assumed to be representative of the soil material used for analysis.

In addition to particle size analysis, other basic properties including soil bulk density, pH, organic carbon, cation exchange capacity, electrical conductivity and clay mineralogy, were determined using standard physical and

Table I. Physico–chemical characteristics of soils measured

Property	Agricultural soil	Mining residue
Texture	Sandy loam	Sandy loam
Sand% (kg kg^{-1})	83·3	89·0
Silt% (kg kg^{-1})	6·6	1·9
Clay% (kg kg^{-1})	10·1	9·1
Clay mineralogy (–)	Kaolinite	Kaolinite–smectite
Specific surface area (m^2 g^{-1})	6·8	12·5
CEC (mmol$_c$ g^{-1})	3·4	8·1
Organic carbon (%)	0·03	8·1
pH (water)	6·1	8·7
Electrical conductivity (μS cm^{-1})	42	380

CEC—cation exchange capacity.

Table II. Some physical characteristics of soils measured [superscripts a and b, respectively, indicate total porosity at the start and at the end (parenthesis) of leaching with 1 mmol l^{-1} NaCl]

Property	Agricultural soil	Mining residue
Bulk density (g cm^{-3})	1·61	1·58
Total porosity (m^3 m^{-3})	0·387[a] (0·354)[b]	0·431[a] (0·417)[b]
	% Sand fraction (kg kg^{-1})	
1000–2000 µm	12·37	1·70
500–1000 µm	26·78	12·81
250–500 µm	21·30	57·46
125–250 µm	15·92	13·67
45–125 µm	2·41	2·40
<45 µm	4·52	1·00

mineralogical methods (Klute, 1986) and are presented in Tables I and II.

Water retention and equivalent pore-size distribution

Soil water retention curves were determined using sintered glass funnels and the Haines method over the low-pressure ranges (Haines, 1923) and pressure plate ceramic membrane apparatus for the higher-pressure range (>60 cm). Air-dried <2 mm soil aggregates were uniformly packed into 3-cm long and 5-cm diameter columns. The column samples were pre-wetted overnight from below to ensure complete saturation. Samples within the columns were confined between coarse sintered glass plates to enhance hydraulic contact, while a 50 µm nylon mesh was placed as filter in both ends of the soil columns. A hanging column experiment was carried out by sequentially imposing the following suctions: 5, 10, 15, 20, 30, 35, 45, 50, 55 and 60 cm. The columns were initially saturated with water by setting the equilibrium at zero suction. The applied suction can be related to an equivalent pore size according to the capillary law for perfectly wettable solids: $\Delta P = (2\sigma/r_p)$, where ΔP is the pressure difference (Pa) across an air–water interface, σ is surface tension of water and air (Jm^{-2}) and r_p is the radius of a circular capillary tube (m). The water retention curve was measured before and after a leaching experiment with different solute concentrations. The porosity and particle size distribution in the effluent before and after leaching with 1 mmol l^{-1} NaCl electrolyte concentration (Table II) were measured to examine changes in pore structure following particle release and re-deposition processes.

Hydraulic conductivity measurements

Laboratory leaching column experiments were carried out to determine saturated hydraulic conductivity using similar columns to those used in the measurement of water retention with soil packed to a bulk density of approximately 1·55 g cm^{-3}. The samples were first purged with carbon dioxide to remove entrapped air, which together with pore blockage play a significant role in controlling flow rates especially in the wetter regime (Wildenschild *et al*., 2001). Samples were saturated overnight in a tray filled with the de-aired solution of known concentration. A Marriotte constant-head device was set up for saturated flow and the soil columns were first leached with an electrolyte concentration of 500 mmol l^{-1} NaCl to a constant flow rate. The solution concentration was then reduced progressively through 500, 100, 50 and 10 to 1 mmol l^{-1} NaCl to assess in detail the dynamics of saturated hydraulic conductivity with time. The saturated hydraulic conductivity (K_s) was estimated for a one-dimensional vertical flow (Klute and Dirksen, 1986).

RESULTS AND DISCUSSIONS

Pore-scale modelling

A three-dimensional model was used by Lehmann *et al*. (2006) to analyse the geometric properties of packed spheres. We used a two-dimensional version of the Lehmann *et al*. (2006) model to characterize the changes in pore space resulting from particle migration within the soil columns during the leaching process.

Modelled size distribution of sand grains

The mass fractions of sand particles with sizes ranging from 45 to 2000 µm were measured in the laboratory. The mass fractions were fitted with a lognormal distribution function denoted as $M(D)$ with the diameter of the sand particle D. The measured and fitted cumulative distribution functions are shown for both soils in Figure 1.

The value of the fitted function $M(D)$ divided by the volume of a sphere with diameter D equals the probability that a sand grain has the diameter D. However, to model the sand grain size in a two-dimensional cross-section, we must determine the diameter d of circular cross-section ('disk') through a medium with spherical particles. Ohser and Mücklich (2002) used Wickell's equation for probability density function to derive the disk diameter distribution function $f(d)$ from the sphere

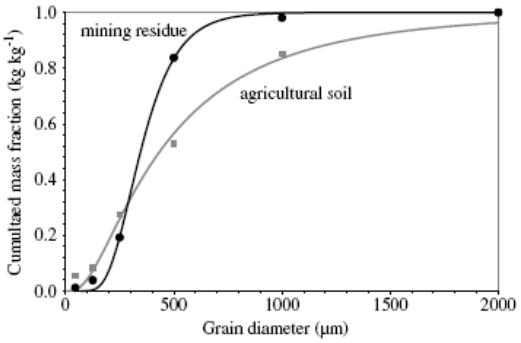

Figure 1. Measured sand size distribution of agricultural soil (grey symbols) and mining residue (black symbols). The measurements are fitted with a lognormal distribution (lines)

diameter distribution in three dimensions $f(D)$:

$$f(d) = \int_d^\infty \frac{d}{\sqrt{D^2 - d^2}} f(D) dD \quad (1)$$

The value $f(d)$ gives the probability that the diameter of a sliced sand grain in the cross-section has the diameter d. By integrating $f(d)$ with respect to the diameter d, we obtain the cumulative distribution function $F(d)$, i.e. the probability that a disk has a diameter smaller than d. By dividing $F(d)$ by $F(d_{\max})$, where $d_{\max}$ is the maximum diameter of 2000 μm, we obtain a number between 0·0 and 1·0. To determine the diameter of a sand particle in the cross-section, a random number n between 0 and 1 is chosen that corresponds to a value of $n = F(d)/F(d_{\max})$ with a disk diameter d.

Modelled coating of sand grains

In the pore-scale model, we assumed that the solid phase consisted of sand grains with a coating containing clay and silt particles. The mass fraction of the clay and silt particles, denoted by c was 0·167 kg kg^{-1} for the agricultural soil and 0·110 kg kg^{-1} for the mining residue. The complementary mass fraction of the sand is denoted by $s = 1 - c$. Initially, all clay and silt particles are modelled as elements of the coating. With changing solute concentration, a fraction ξ of these particles is released. By defining the cross-section of the bare sand particles per total cross-section as Φ (m^2 m^{-2}), the fraction of the coating is $\Phi(1-\xi)c/s$ and the fraction of released particles is $\Phi\xi c/s$. The sum of the solid fractions is complementary to the porosity ϕ (m^2 m^{-2})

$$\Phi + \frac{(1-\xi)c}{s}\Phi + \frac{\xi c}{s}\Phi = 1 - \phi \quad (2)$$

Owing to the instability of the coating, the parameters ξ, ϕ, and Φ are not constant but solute-concentration dependent. For example, the porosity ϕ decreased from 0·387 m^2 m^{-2} to 0·354 m^2 m^{-2} for the agricultural soil and from 0·431 m^2 m^{-2} to 0·417 m^2 m^{-2} for the mining residue owing to decreasing solute concentration.

To mimic the experimental conditions, we took into account the fact that the release of particles may be different for the two media and modelled this process using experimental data. The mass of colloids in the effluent, η, was determined experimentally as 0·068 mg for the agricultural soil and 0·083 mg for the mining residue. Assuming that the ratio of colloids in the effluent of the agricultural soil and the mining residue corresponds to the ratio of the particle release, we propose the following equation:

$$\frac{\eta_A}{\eta_M} := \alpha = \frac{\frac{\xi_A c_A}{s_A}\Phi_A}{\frac{\xi_M c_M}{s_M}\Phi_M} \Rightarrow \xi_A = \alpha \xi_M \frac{c_M s_A}{s_M c_A}\frac{\Phi_M}{\Phi_A} \quad (3)$$

where $\eta_A/\eta_M = \alpha$ is the effluent mass ratio of the two media and the subscripts $_A$ and $_M$ denote respectively agricultural soil and mining residue.

Here, we do not discuss the process of particle release as a function of solute concentration. Instead, we describe the change of the pore structure if a certain amount of fine particles are released and are re-deposited. The parameter ξ_M was varied from 0 to 0·1, corresponding to a maximum release of 10% of the coating in case of the mining residue and for the agricultural soil, ξ_A was calculated using Equation (3).

Spatial distribution of coated sand grains

As discribed in subsection *Modelled size distribution of sand grains*, the size of particle i was determined by choosing a random number between 0 and 1 and numerically solving the equation $n_i = F(d_i)/F(d_{\max})$ for the disk diameter of the sand grain d_i. Owing to the coating with clay and silt particles, the cross-section of the coated particles must be increased. With the concentration-dependent coating, the diameter is increased according to

$$\left(\frac{d_i + d_{C_i}}{d_i}\right)^2 \Rightarrow 1 + \frac{(1-\xi)c}{s} \quad (4)$$

with the thickness of the coating of the particle d_{c_i}.

The creation of new particles, i.e. the determination of disk diameter, is repeated as long as the following criterion is fulfilled:

$$\sum_i 1/8(d_i + d_{C_i})^2\pi < L^2(1-\phi) \quad (5)$$

with the cross-section of the coated particles at the left and the area of the solid phase at the right side, where L (m) is the size of the system.

In the next step, the disk sizes are sorted and random positions for the centres of the disks are chosen, beginning with the largest disk diameters. In case of overlapping, new random positions are chosen. The resulting modelled media are shown in Figure 2.

Discretization of modelled cross-sections

To quantify the pore geometry of the generated media, the cross-section is segmented into an image with pixels determined as grains or pore spaces. For that purpose, a quadratic cross-section of the medium with size $L =$ 7·5 mm was subdivided into 750 × 750 elements of size 0·01 mm. For each element of the image, denoted as a pixel, the fraction of solid grain was determined. All pixels with a fraction of solids below a threshold were determined as pores. The threshold was chosen according to the requirement that the fraction of the coated sand grains in the image equals the measured fraction $\Phi + \Phi(1-\xi)c/s$. To model the re-deposition of the colloids, pixels of the pore space are chosen randomly and determined as deposited colloids. The number of deposited colloids N is given by:

$$N = \frac{\xi c}{s}\Phi\left(\frac{L}{\Delta x}\right)^2 \quad (6)$$

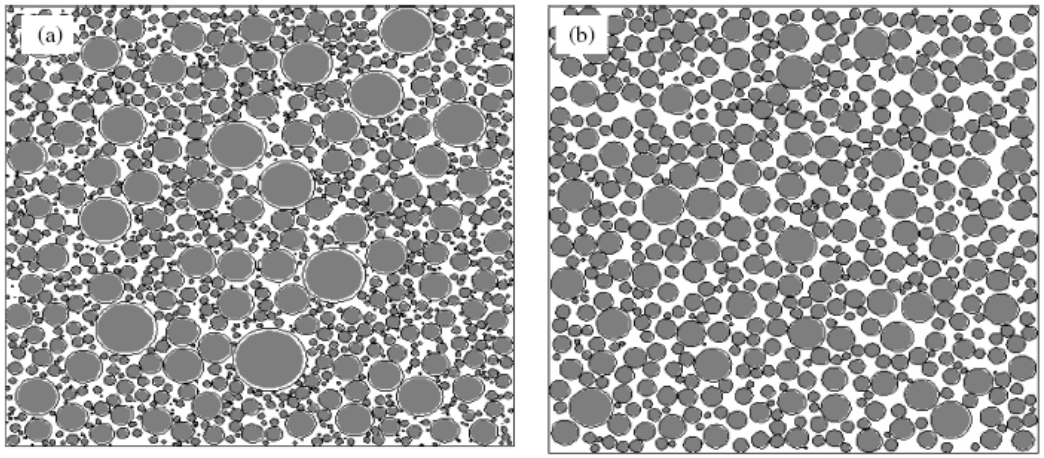

Figure 2. Modelled cross-section of the agricultural soil (a) and the mining residue (b). Sand particles (grey) are coated with a layer containing clay and silt particles. In the case of the agricultural soil, the clay and silt contents are higher as indicated with the thicker layer

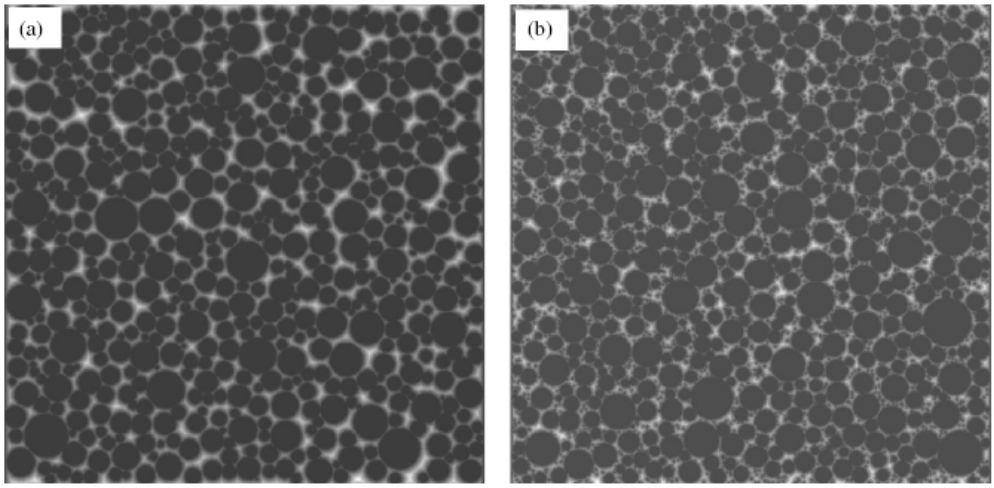

Figure 3. Effect of clay re-arrangement on the distance transform of the mining residue. Bright or white colour indicates a distance from the solid phase (in black). In Figure 3(a), the coating is intact. In Figure 3(b), 3590 particles are re-deposited and reduce the distance between pores and solid phase

where $\Delta x = 0{\cdot}01$ mm is the pixel size. The maximum number of re-deposited particles was 3590 corresponding to 0·64% of the total cross-section of the medium.

Quantification of pore size

Hydraulic properties such as water retention and saturated hydraulic conductivity depend on the size of the pores. To determine the pore sizes, the distance from the solid phase is determined in the first step for all pixels of the pore space. This size corresponds to the radius of a disk that lies entirely within the pore space. A value equal to the diameter of such a disk (denoted as distance transform) is attributed to the pixels of the pore space. The distance is shown in Figure 3.

The centre of a small disk close to the solid wall may be in the periphery of a larger disk. In such a case, the size of the larger disk is attributed to the pixel close to the solid wall. This maximum size for each pixel of the pore space is denoted as pore size. The pore sizes in the cross-sections are shown in Figure 4.

The pore sizes and the distances from the solid phase are affected by the re-deposition of particles. We now quantify the effect of re-deposition on the pore size and distance.

Measured effects of pore structure dynamics on hydraulic properties. Figure 5 shows the size distribution of the particles in the effluent from the 1 mmol l^{-1} NaCl leaching. The majority of particles lie in the size range of 0–15 μm. This effluent size distribution provides insights into the size range of particles involved in particle migration during leaching which causes changes in hydraulic properties. The effect of particle migration is reflected by changes in the water retention characteristic

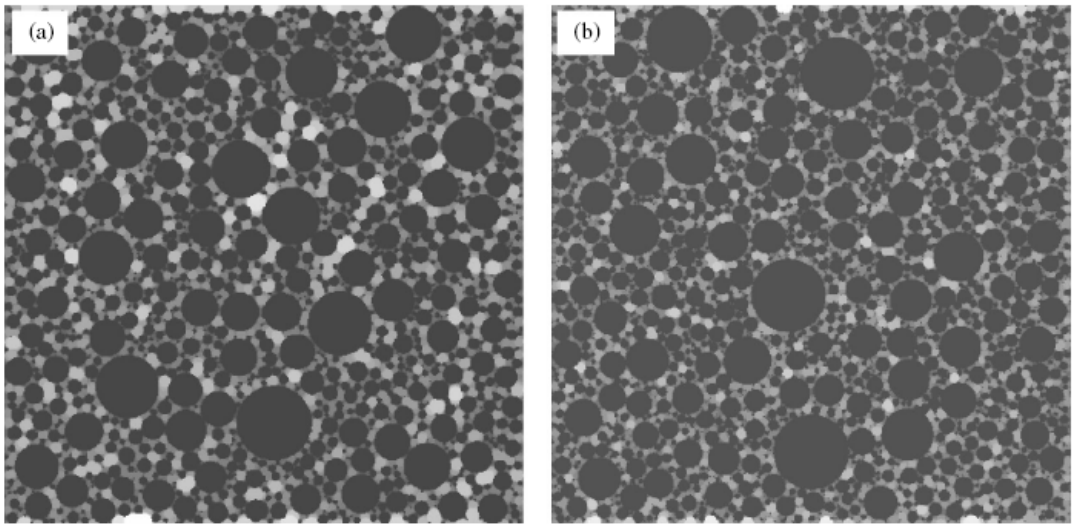

Figure 4. Effect of clay re-arrangement on the pore sizes of the agricultural soil. Particles are shown in black and large pores in white. In Figure 4(a), the coating is intact and the system contains less but larger pores. In Figure 4(b), 2948 particles are re-deposited dividing large pores into more smaller units

curves (Figure 6) that can be interpreted as a shift in the distribution function of equivalent pore sizes (Figure 7). The arrows in Figure 6 indicate the air-entry values.

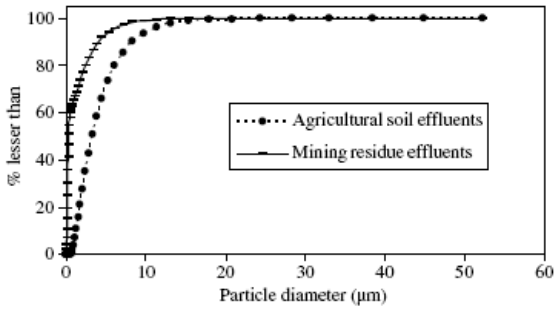

Figure 5. Particle size distribution of effluent or migrating particles

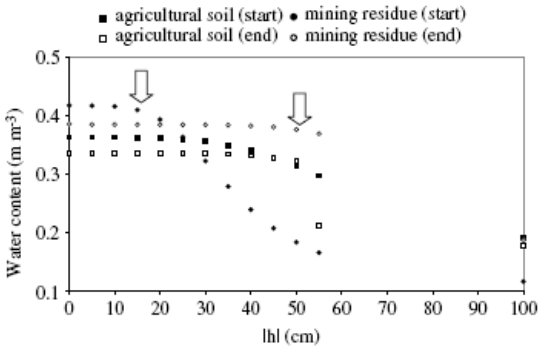

Figure 6. Measured soil water retention curves. During the experiments with decreasing solute concentration, the porosities decrease. The arrows indicate the air-entry values. In case of the mining residue, the water retention curve is shifted to higher absolute values of matric potential head

In the case of the mining residue, the water retention curve shifted to higher absolute values of matric potential head. In the same figure, a decrease of porosities following the leaching of soil columns is shown. This decrease in porosity is attributed to pore clogging owing to particulate entrapment. This clogging reduced the permeability of the soil. The measured saturated hydraulic conductivities for both soils are shown in Figure 8 and indicate a decrease of saturated hydraulic conductivity with reduced concentration. This was attributed to a decreased fraction of large pores after deposition and re-deposition of colloidal particles. With decreasing solute concentration, clay and silt particles are released from the coating and are re-deposited in the pore space. The decrease was most pronounced in the case of the mining residue.

Modelling the pore structure dynamics and its effect on the hydraulic properties. We now examine the ability of the proposed pore structure model to describe changes in hydraulic properties. In the model, rearranged particles were placed randomly in the pore space leading to a change in the distance transform and the pore-size distribution. In Figure 9, the effect of increasing particle release on pore size and distance transform is shown. The number of rearranged particles increased from 0 to a maximum value of 3590. For both soils, modelling results have revealed that the fraction of large pores is reduced and this was reflected by a decreased hydraulic conductivity (Figure 8), because the flow increases to the power of four with the pore radius. The trends for the mode, i.e. the maximum of the pore-size distribution, are different for the two soils. For the agricultural soil, the mode occurs at 45 μm in all cases. In the case of the mining residue, the mode shifted from about 75–95 μm for intact coatings to smaller values of 45 μm for the

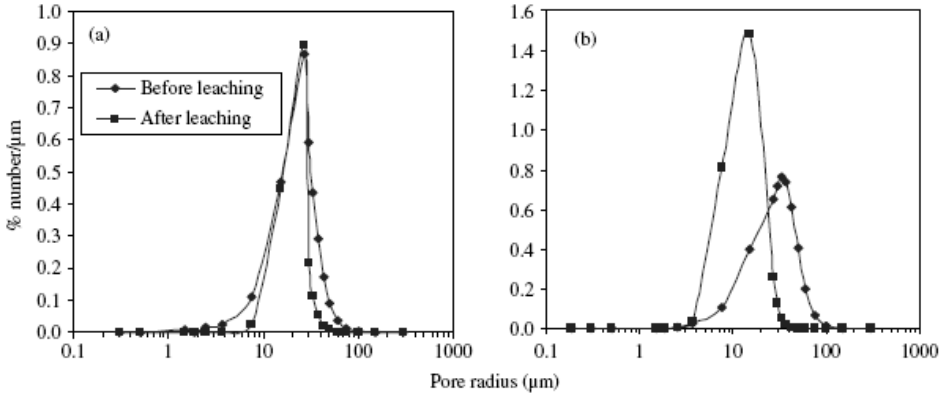

Figure 7. Changes of pore-size distribution owing to particle re-arrangement: (a) agricultural soil, and (b) mining residue

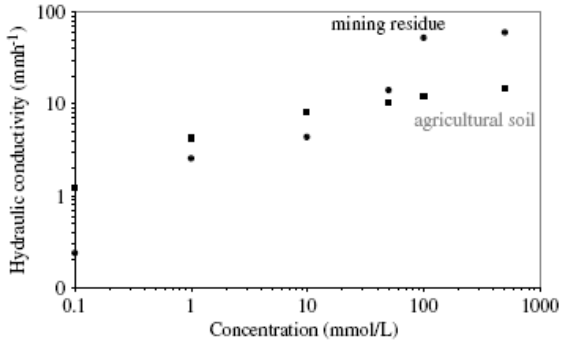

Figure 8. Hydraulic conductivity as a function concentration during leaching for agricultural soil and mining residue

situation with released particles. This shift of the mode of the modelled pore-size distribution corresponds to the shift of the measured air-entry value of the water retention curves.

To examine this feature in more detail, we have to distinguish between the water retention curve and the true geometric pore-size distribution function. Using the capillary law, an equivalent pore size can be attributed to the absolute value of the matric potential head h. Thus, the cumulative size distribution of these equivalent pore sizes equals the water retention curve. However, the equivalent pore size is not the same as the geometric size of a pore owing to the connectivity of the pore network. For example, the drainage of a large pore surrounded by small pores is controlled by the drainage of the small pores. The equivalent pore size determined with the measured water retention function will be the same for the enclosed large and the surrounding small pores.

To compare the water retention curve with the modelled geometric pore-size distribution, the mode of the distribution function is more important than the size of the largest pores. The set of pixels with a pore size r that is larger than the mode of the distribution function r_m is small and does not build a connected network that spans the whole system. Air entry will occur if all pore pixels of size $r \geq r_t$ form a connected system and the applied suction exceeds the capillary forces in a pore of size r_t. Because the pores of size $r = r_m$ are the most frequent in the cross-section, the set of pixels with size $r \geq r_m$ becomes more connected. In Figure 10, the cross-sections are shown for different r_t for the agricultural soil before and for the mining residue after the re-deposition. Note that the relevant connectivity in three dimensions cannot be shown in two-dimensional cross-sections. However, we can see that in the cross-sections for $r_t = r_m = 45$ µm, corresponding to the mode of the pore-size distribution, large connected clusters emerge. So, air is expected to enter the pore space if the applied hydraulic head is strong enough to exceed the capillary forces in pores of size r_m.

SUMMARY AND CONCLUSIONS

Using the model of pore structure proposed by Lehmann *et al*. (2006), we have been able to explain the measured effects of particle deposition on the hydraulic properties. Comparing the modelled pore-size distribution with the measured water retention curves for the four cases, (i) agricultural soil before the release process, (ii) mining residue before the release, (iii) agricultural soil after the re-deposition and (iv) mining residue after the re-deposition, the measured water retention curves were very similar for the cases (i), (iii) and (iv). The air-entry values of these three curves were 2–3 times the value observed for the mining residue before the release process (ii). The same phenomenon was simulated with the pore model: the mode of the modelled pore-size distribution was at 45 µm for (i), (iii) and (iv) and about 75–95 µm for (ii). The ratio of the capillary forces associated with these values of the modes is equal to 1·67 to 2·11 and is similar to the measured ratio of the air-entry values.

Apart from the shift of the water retention curve in the case of the mining residue, we found a substantial decrease in measured saturated hydraulic conductivity for both soils. This decrease could be explained with the modelled destruction of large pores owing to particle re-deposition. The decrease of saturated hydraulic conductivity (59·95–0·24 mm h^{-1}) was more pronounced in the case of the mining residue. The tremendous change of the hydraulic properties in the case of the mining

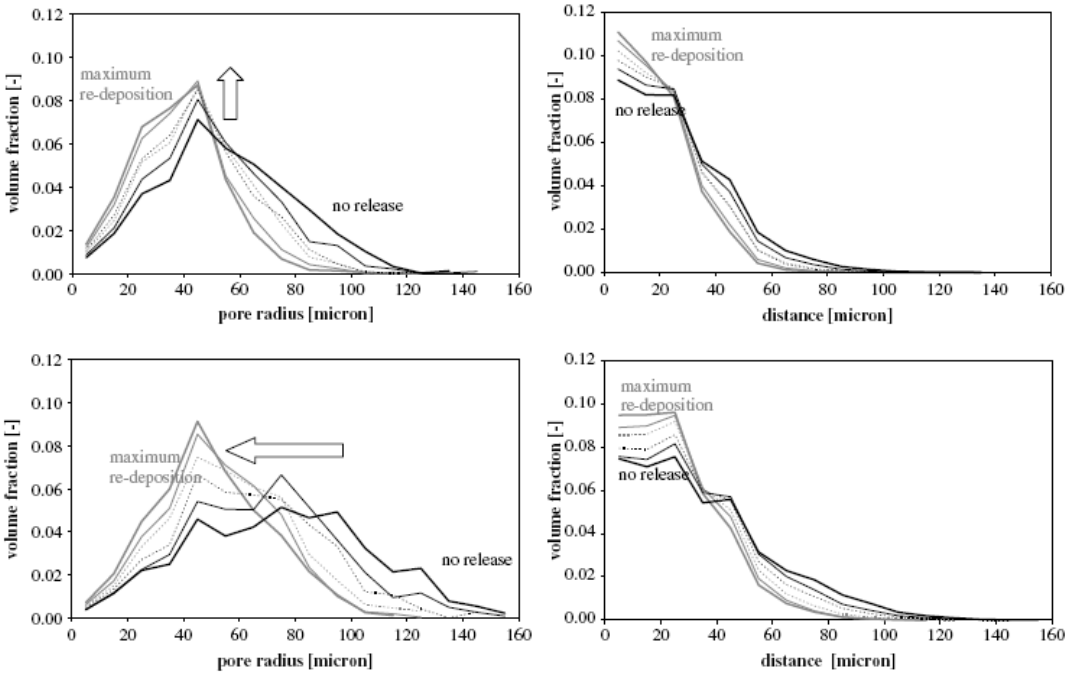

Figure 9. Computed distribution of pore sizes (left) and distance from solid phase (right) as a function of re-disposition. The results for the agricultural soil are shown on top and at the bottom for the mining residue. With increasing deposition, large pores are replaced by smaller voids. In case of the mining residue, the position of the mode of the pore-size distribution is shifted to smaller sizes, resulting in a changed water retention curve. The number of released particles changed from 0 to a maximum value of 3590

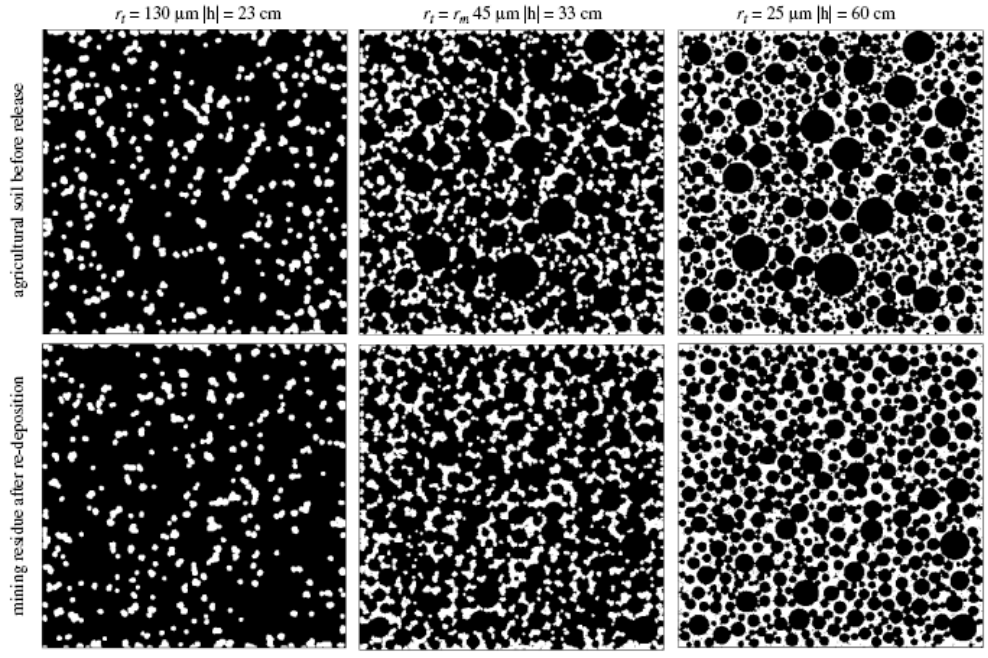

Figure 10. Size-dependent pore connectivity for the agricultural soil and the mining residue. All particles and pores smaller than the threshold value r_t, are shown in black and pores of radius $r \geq r_t$ in white. With decreasing threshold radius, the system of pores becomes more continuous. The mining residue after the re-deposition has similar properties as the agricultural soil before the release process

residues is caused by a shift of the pore-size distribution function to smaller values with decreasing solute concentration. Initially, the pore-size distribution was flat with a wide range of pore sizes. This curve is shifted to smaller sizes with a more narrow size distribution. For the agricultural soil, there was little shift of the water retention curve detected with appreciable decrease of the saturated hydraulic conductivity (14·64–1·24 mm h^{-1}). This is attributed to localized pore clogging (similar to a surface seal) affecting saturated hydraulic conductivity, but not the microscopically measured pore-size distribution or water retention.

REFERENCES

Arya LM, Ley FJ, Shouse PJ, van Genuchten MTH. 1999b. Relationship between the hydraulic conductivity function and the particle size distribution. *Soil Science Society of America Journal* **63**: 1063–1070.

Assouline S, Tessier D, Bruand A. 1998. A conceptual model of the soil water retention curve. *Water Resources Research* **34**: 223–231.

Auset M, Keller AA. 2004. Pore-scale processes that control dispersion of colloids in saturated porous media. *Water Resources Research* **40**: W03503.

Bronick CJ, Lal R. 2005. Soil structure and Management: a review. *Geoderma* **124**: 3–22.

Day PR. 1965. Particle fractionation and particle-size analysis. In *Methods of Soil Analysis Part I'. Agronomy 9*, Black CA (ed). America Society of Agronomy: Madison, WI; 545–567.

FAO. 1998. *World Reference Base for Soil Resources*, *World Soil Resources Report 84*. Food and Agriculture Organization of the United Nations: Rome.

Fischer U, Celia MA. 1999. Prediction of relative and absolute permeabilities for gas and water from soil water retention curves using a pore scale network model. *Water Resources Research* **35**: 1089–1100.

Grolimund D, Elimelech M, Borkovec M, Barmettler K, Kretzschmar R, Sticher H. 1998. Transport of in situ mobilized colloidal particles in packed soil columns. *Environmental Science & Technology* **32**: 3562–3569.

Haines WB. 1923. The volume changes with variations of water content in soil. *Journal of Agricultural Science* **13**: 296–310.

Huang G, Zhang R. 2005. Evaluation of soil water retention curve with the pore-solid fractal model. *Geoderma* **127**: 52–61.

Hunt AG, Gee GW. 2002a. Application of critical path analysis to fractal porous media: Comparison with examples from the Hanford site. *Advances in Water Resources* **25**: 129–146.

Hunt AG, Gee GW. 2002b. Water-retention of fractal soil models using continuum percolation theory: tests of hanford site soils. *Vadose Zone Journal* **1**: 252–260.

Hwang SI, Powers SE. 2003. Using particle-size distribution models to estimate soil hydraulic properties. *Soil Science Society of America Journal* **67**: 1103–1112.

Kay BD. 1998. Soil structure and organic carbon: a review. In *Soil Processes and the Carbon Cycle*, Lal R, Kimble JM, Follett RF, Stewart BA (eds). CRC Press: Boca Raton, FL; 169–197.

Klute A. 1986. *Methods of Soil Analysis "Part 1–Physical and Mineralogical Methods*, *Agronomy No. 9*, 2nd edn, Klute A (ed.). American Society of Agronomy: Madison, WI.

Klute A, Dirksen C. 1986. Hydraulic conductivity and diffusivity: laboratory methods. In *Methods of Soil Analysis (1986). "Part 1–Physical and Mineralogical Methods*, *Agronomy No. 9*, 2nd edn, Klute A (ed.). American Society of Agronomy: Madison, WI.

Kravchenko A, Zhang R. 1998. Estimating the soil water retention from particle size distributions: a fractal approach. *Soil Science* **163**: 3171–3179.

Kretzschmar R, Borkovec M, Grolimund D, Elimelech M. 1999. Mobile subsurface colloids and their role in contaminant transport. *Advances in Agronomy* **66**: 121–194.

Lebron I, Robinson DA. 2003. Particle size segregation during hand packing of coarse granular materials and impacts on local Pore-scale structure. *Vadose Zone Journal* **2**: 330–337.

Lebron I, Suarez DI, Yoshida T. 2001. Gypsum effect on the aggregate size and geometry of three soidic soils under reclamation. *Soil Science Society of America Journal* **66**: 92–98.

Lehmann P, Wyss P, Flisch A, Lehmann E, Vontobel P, Kaester A, Beckmann F, Frey O, Gygi A, Flühler H. 2006. Tomographical imaging and mathematical description of porous media used for the prediction of fluid distribution. *Vadose Zone Journal* 5: 80–97 DOI:10.2136.

Leij FJ, Ghezzehei TA, Or D. 2002. Analytical models for soil pore-size distribution after tillage. *Soil Science Society of America Journal* **66**: 1104–1114.

Malvern Instruments Ltd. 1995. Malven Mastersizer ver 2·18.

Ohser J, Mücklich F. 2002. *Statistical Analysis of Microstructures in Materials Science*. John Wiley and Sons: New York.

Pachepsky YA, Rawls WJ. 2003. Soil structure and pedotransfer functions. *European Journal of Soil Science* **54**: 443–451.

Ranville FJ, Chittleborough DJ, Beckett R. 2005. Particle-size and elemental distributions of soil colloids: implications for colloid transport. *Soil Science Society of America Journal* **69**: 1173–1184.

Reddi LN, Ming X, Hajra MG, Lee InMo. 2000. Permeability reduction of soil filters due to physical clogging. *Journal of Geotechnical and Geoenvironmental Engineering* **126**: 236–246.

Soil Survey Staff. 1996. *Keys to Soil Taxonomy*, 7th edn. United States Department of Agriculture: Washington, DC.

Stokes GG. 1891. *Mathematical and Physical Papers III*. Cambridge Press: Cambridge.

Tuller M, Or D. 2002. Unsaturated hydraulic conductivity of structured porous media: review of liquid configuration-based models. *Vadose Zone Jounal* **1**: 14–37.

Vogel HJ. 2000. A numerical experiment on pore size, pore connectivity, water retention, permeability, and solute transport using network models. *European Journal of Soil Science* **51**: 99–105.

Vogel HJ, Roth K. 2001. Quantitative morphology and network representation of soil pore structure. *Advances in Water Resources* **24**: 233–242.

Wildenschild D, Hopmans JW, Simunek J. 2001. Flow rate dependence of soil hydraulic characteristics. *Soil Science Society of America Journal* **65**: 35–48.